Modified Gerchberg–Saxton algorithm to generate vector beams

Author: Inés Fernández Menéndez, ifername10@alumnes.ub.edu
Facultat de Física, Universitat de Barcelona, Diagonal 645, 08028 Barcelona, Spain.

Advisor: David Maluenda Niubó, dmaluenda@ub.edu

Abstract: This study explores the generation of vector beams using a modified Gerchberg-Saxton (GS) algorithm in the context of computer-generated holography (CGH). The objective is to reconstruct two orthogonal electric field components with predefined intensity profiles and relative phase distribution between components. The methodology involves applying the GS algorithm independently to each component while imposing their relative phase, allowing the global phase to evolve freely. The vector beams generated are Laguerre-Gaussian beams with varying topological charges, and the holograms are computed for three different cases. The results show successful convergence in the central regions of the beams despite the presence of speckle-like noise. The polarization pattern follows the expected behavior, which means that the relative phase is well reconstructed. Metrics such as similarity and phase error confirm the algorithm's convergence. These results check the viability of the method to be experimentally implemented, as they are computed according to the laboratory conditions.
Keywords: Gerchberg-Saxton algorithm, computer-generated holography, polarization, phase retrieval.
SDGs: This work is related to the sustainable-development goals SDG 4

I. INTRODUCTION

Holography is a technique that enables a wavefront to be recorded and later constructed. Traditionally, holograms are recordings of an interference pattern that reproduces a light field using diffraction [1]. However, we will compute the hologram knowing the mathematical relation of the light field on two different planes [2]. In our case, we will work with Fraunhofer's diffraction, which is achieved by making the distance between the image and diffraction plane tend to infinity or by being at a lens' focal plane. This setup ensures that the relation between the fields in these two planes is a Fourier transform.

In 1971, R.W. Gerchberg and W.O. Saxton proposed an algorithm for determining the complete wave function from intensity recordings in the image and diffraction planes, allowing us to solve the phase problem (problem based on the loss of information about the phase when making a physical measurement) and to determine the phase of the complete wave function whose intensity (the amplitudes are proportional to the square roots of the measured intensities), in the imaging and diffraction planes, is known [3].

Computer-generated holography (CGH) is a technique that uses computational algorithms to generate holograms by generating holographic interference patterns. A computer calculates a holographic pattern that is used to set the optical properties of a spatial light modulator (SLM) that then diffracts the read-out light wave to yield the desired optical wavefront [2]. A CGH is a complex wavefront processor. In the CGH are specified an incoming wavefront description as well as the desired diffracted wavefront, or part of it, in the near or far field. Once we have this, the task is to find the best phase (or amplitude) mapping that will perform the diffraction job in an acceptable way considering the requirements imposed [4]. Compared to classical optical holography, CGH does not require a real object, since the hologram can be generated by computing the light field in the far observer plane and transforming it to the lens plane using the Fourier transform [2].

CGH aims to determine the phase that must be added to a plane wavefront (from a laser) so that, upon diffraction, it yields the desired intensity distribution. This process is essentially the same as the Gerchberg-Saxton algorithm. The only difference is that the intensity in the diffraction plane is not measured but imposed as a target, and the estimated phase is the computer-generated hologram.

Computer-generated holograms are powerful tools for digitally encoding phase or amplitude information to reconstruct optical wavefronts. One of its implementations is their application to plane wavefronts, which can be modulated using parallel-aligned liquid crystal displays (LCD-PA). This devices consist of an array of liquid crystal (a phase between solid and liquid) cells with molecules aligned (regularly) in parallel and, when properly polarized, they can control the optical path of light waves (spatial light modulators) and the phase of light passing through each cell without significantly affecting its amplitude (phase-only modulators). A CGH can be computed and loaded onto the LCD-PA. When illuminated by a plane wave (as a laser beam), the phase modulation introduced by the CGH produces a diffracted wavefront that reconstructs the optical field [4], [5], [6].

In this paper, we study vector beams, fully polarized beams that show different polarization states at different local positions on the detector plane [7] (i.e.,beams

with a non-uniform polarization distribution). These beams offer advantages over scalar beams (uniform polarization) in the focal region, particularly in applications such as microscopy or particle trapping [8], [9]. A non-homogeneous polarization distribution requires different intensity profiles in two transverse and orthogonal components. Moreover, the phase distribution between these two components plays a crucial role in the overall polarization distribution.

The aim of this study is to implement two Gerchberg-Saxton algorithms, one for each electric field component, connected through the imposed relative phase. This approach allows for the reconstruction of two predefined target intensity profiles and the relative phase between them, leaving the global phase as a degree of freedom that enables convergence.

The structure of this paper is as follows. First, we review the foundations of the GS algorithm and the vector beams used in this work. Then, we introduce the modified Gerchberg-Saxton algorithm used in our approach. Finally, we present the results obtained and a discussion of their physical implications.

II. METHOD

A. The Gerchberg-Saxton algorithm

The Gerchberg-Saxton algorithm [3] is an iterative algorithm that lets us determine the phase of a wavefront from the intensity in two planes. Since both planes are related by the Fourier transform, by only one phase distribution, we obtain the phase distribution in the other plane.

The algorithm begins (Figure 1) with the complex wave function in the entrance pupil plane (EP plane) of a diffraction system, such as a lens (assigning a random phase in the interval $[-\pi, \pi]$ that serves as an initial estimate of the phase). A Fourier transform is applied to obtain the wavefunction on the diffraction plane. Once in this plane, we impose the amplitude and perform an inverse Fourier transform imposing again the known amplitude on the EP plane. After this, the process is repeated.

Throughout this procedure, we retain the phase information and let it evolve with the Fourier transform.

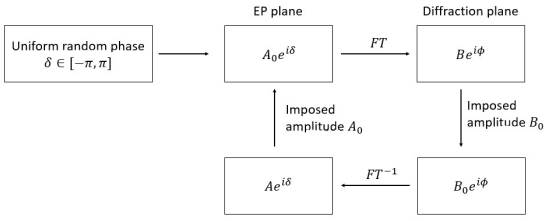

FIG. 1: Representation of the Gerchberg-Saxton algorithm where FT stands for Fourier transform.

B. Laguerre-Gaussian beam

A Gaussian beam is a beam whose amplitude envelope in the transverse plane is given by a Gaussian function, which also implies a Gaussian intensity profile. Gaussian beams are the lowest-order transverse mode solutions of the Helmholtz equation (if we describe an electromagnetic wave as a field $u(x, y, z; t) = U(x, y, z)e^{-iwt}$, $\nabla^2 U + k^2 U = 0$ with $k = \frac{w}{c} = \frac{2\pi}{\lambda}$). From the Helmholtz equation we get the paraxial wave equation, by introducing $U(x, y, z) = u(x, y, z)e^{-ikz}$ and the paraxial assumption $\frac{\partial^2 u}{\partial z^2} = 0$,

$$\nabla^2 u - 2ik\frac{\partial u}{\partial z} = 0. \tag{1}$$

By solving it in different coordinate systems with different symmetry assumptions, we can define different beams (higher-order modes) [10].

In our experimentation, we will study Laguerre-Gaussian (LG) beams that are a family of orthogonal basis sets with different radial (labeled with $p \geq 0$) and azimuthal (labeled with $l \in \mathbb{Z}$) modal numbers (LG beams are vortex beams). These functions are written in cylindrical coordinates using generalized Laguerre polynomials.

$$LG_{pl}(\rho, \phi, z) = C_{pl}^{LG} \frac{1}{w(z)} \left(\frac{\rho\sqrt{2}}{w(z)}\right)^{|l|} L_p^{|l|}\left(\frac{2\rho^2}{w^2(z)}\right) \times \\ \times e^{\left[-\frac{\rho^2}{w^2(z)} - ik\frac{\rho^2 z}{2(z^2+z_R^2)}\right]} e^{il\phi} e^{i\psi(z)}, \tag{2}$$

where $w(z) = w_0\sqrt{1 + z/z_R}$ is the beam radius, $\psi(z) = (|l| + 2p + 1)\arctan\left(\frac{z}{z_R}\right)$ with z_R the Rayleigh distance and C_{lp}^{LG} is the normalization constant [11]

$$C_{pl}^{LG} = \sqrt{\frac{2p!}{\pi(p + |l|)!}}. \tag{3}$$

C. Modified GS algorithm

In this work, we are interested in, based on the algorithm above-mentioned, generating specific vector beams by imposing a defined amplitude and relative phase between the components of the field in the respective planes, allowing the wave functions to evolve and converge toward a desired polarization.

In the diffraction plane, we impose a field with the LG_{01} mode (characterized by its donut shaped distribution) and $z = 0$, so we get two components for the electric field given by

$$E_x(\rho, \phi) = \sqrt{\frac{2}{\pi}}\frac{1}{w_0}\left(\frac{\sqrt{2}\rho}{w_0}\right) e^{-\frac{\rho^2}{w_0^2}} \sin(m\phi), \\ E_y(\rho, \phi) = \sqrt{\frac{2}{\pi}}\frac{1}{w_0}\left(\frac{\sqrt{2}\rho}{w_0}\right) e^{-\frac{\rho^2}{w_0^2}} e^{in\phi} \cos(m\phi), \tag{4}$$

where each component comes from the inclusion of the angular dependence of the field (ϕ represents the angular coordinate), where n is the topological charge on the relative phase distribution and m is the corresponding topological charge affecting the amplitude. These two free parameters let us define different beams to be explored.

The relative phase of the target δ is computed from the complex comparison of both components in Eq. (4). Then, every Fourier transform step on the GS algorithm returns a couple of phases δ_x and δ_y corresponding to each component. This results in a phase error expressed as $\epsilon = [(\delta_y - \delta_x) - \delta]$. This error is equally compensated for in the retrieved phases to ensure that the relative phase is now imposed, while the global phase is left as a freedom degree to allow convergence.

$$\delta_x \to \delta_x + \frac{\epsilon}{2}; \quad \delta_y \to \delta_y - \frac{\epsilon}{2}. \tag{5}$$

In the EP plane, we impose an amplitude distribution of 0's and 1's representing the profile of the entrance pupil, while the phase is evolving during the iterations.

III. RESULTS

Throughout our experimentation, we have studied three types of beams, from which different results can be analyzed. We have imposed different values for the parameters m and n in Eq. (4). In other words, the beams have been modified by altering either their phase or their amplitude to explore the viability and performance of the method.

A. Conventional azimuthally polarized beam

The first beam under study is the conventional donut-mode azimuthally polarized beam, corresponding to a two lobes profile for each component and the relative phase changing with the cartesian quadrants ($m = 1$ and $n = 0$ in Eq. (4)). Once we impose these conditions and execute the algorithm, we obtain Figure 2.

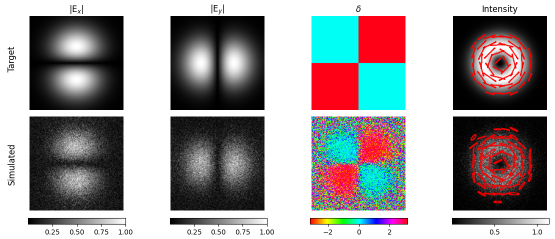

FIG. 2: Representation of the electric field components (first two columns), relative phase between the electric field components (third column) and total intensity of the beam, along with the polarization ellipses (last column) imposed in the diffraction plane as our target (first row) and after executing the Gerchberg-Saxton algorithm (second row).

By examining both rows, we observe that the simulation does not give identical patterns. However, in the central regions of the images, where the intensity is higher, we obtain good approximations. The regions with low intensity (peripheral regions) have minimal impact on the result. Taking this into account, the presence of noise increases toward the edges of the images.

B. Four lobes azimuthally polarized beam

The second beam under study corresponds to a four lobes profile for each component and a relative phase in quadrants just like before ($m = 2$ and $n = 0$). Once we impose these conditions and execute the algorithm, we obtain Figure 3.

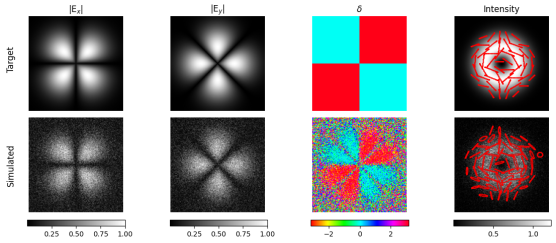

FIG. 3: Representation of the electric field components (first two columns), relative phase between the electric field components (third column) and total intensity of the beam, along with the polarization ellipses (last column) imposed in the diffraction plane as our target (first row) and after executing the Gerchberg-Saxton algorithm (second row).

C. Donut beam with azimuthal relative phase

The last beam under study is generated by imposing a relative phase corresponding to the angular polar coordinate with two electric field components defined by Eq. (4) imposing $m = 1$ and $n = 1$. Once we impose these conditions and execute the algorithm, we obtain the following.

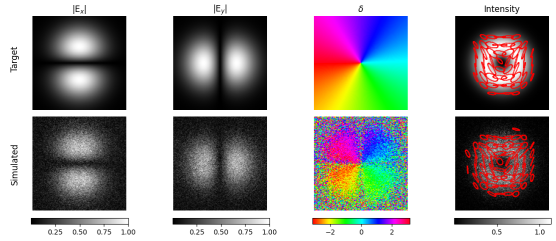

FIG. 4: Representation of the electric field components (first two columns), relative phase between the electric field components (third column) and total intensity of the beam, along with the polarization ellipses (last column) imposed in the diffraction plane as our target (first row) and after executing the Gerchberg-Saxton algorithm (second row).

IV. DISCUSSION

Based on the results presented in Section III and, observing Figures 2, 3, and 4, a consistent behavior is observed in the reconstructed patterns we have studied.

We can observe that the reconstructed (or simulated) pattern (second row in our figures) is highly similar to the initial configuration or our target (first row) despite the presence of speckle-like noise. This speckle noise is mainly due to destructive interferences between adjacent sampling points in the EP plane [12].

Even so, the phase (third column) converges toward our initial conditions as it has a tendency to the imposed polarization in each case. In particular, the central region of the image has the expected behavior, although the presence of noise must be taken into consideration (the edges exhibit significant noise but little intensity, and therefore have minimal impact on the result). Moreover, in the central region we can observe regions where the expected relative phase is not achieved. This behavior can be attributed not only to the noise, but also to the fact that in regions where one of the electric field components is zero, the relative phase between them is undefined (it becomes linear polarization associated with the non-zero component).

In terms of the polarization ellipses (last column), they reflect the relative phase introduced between the electric field components. The ellipse is a horizontal line in regions where the y-component of the electric field is zero, and a vertical line where the x-component is zero. Between these extremes, the ellipses evolve following the Polarization Ellipse Equation (Eq. (6)) which is the equation of an ellipse that refers to polarized light (δ is the relative phase between the two components) [13].

$$\frac{E_x(z,t)^2}{E_{0x}^2} + \frac{E_y(z,t)^2}{E_{0y}^2} - \frac{2E_x(z,t)E_y(z,t)}{E_{0x}E_{0y}}\cos\delta = \sin^2\delta. \tag{6}$$

In all three cases, the polarization ellipses obtained tend to follow the expected behavior, but they do not exactly match the expected patterns, due to the presence of speckle noise.

To further study the effectiveness of our approach, we analyze similarity, a metric to measure how similar two images are [14]. In our case, we compare the electric field amplitude distributions before and after implementing the algorithm (i.e., the similarity between the images in the first and second row for the two first columns). Regarding the phase, we can study the evolution of the averaged phase error, ϵ.

For the three cases analyzed, we observe that, as we anticipated, the presence of noise results in two images that aren't (in terms of the similarity) highly similar (we obtain small values for the similarity, both for the x and y-components). However, in terms of convergence, the similarity stabilizes after the second iteration with little fluctuations. We observe that the x-component of the electric field exhibits a greater similarity than the y-component in the cases $m = 1$, $n = 1$ and $m = 2$, $n = 0$, and a similar trend for both components in the case $m = 1$, $n = 0$.

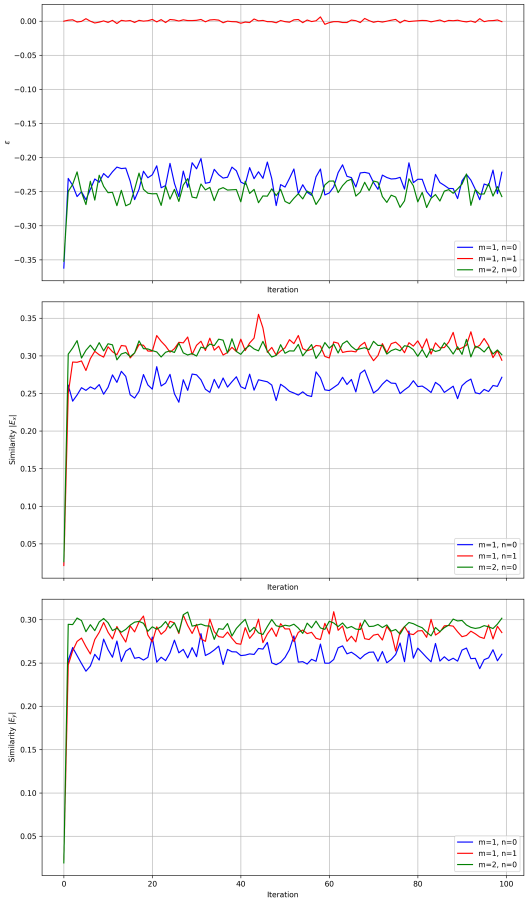

FIG. 5: Representation of the first 100 iterations of the phase error, $\epsilon = [(\delta_y - \delta_x) - \delta]$, where δ is the imposed relative phase (first) and the similarity of the electric field components (x-component, second and y-component, third) for the three beams we have studied in Section III (blue is $m = 1$, $n = 0$; red is $m = 1$, $n = 1$; green is $m = 2$, $n = 0$).

Regarding the phase, the evolution of ϵ shows a similar trend, with values oscillating within a specific range. The smallest phase error, corresponding to the lowest value of $|\epsilon|$, is observed in the simulation for $m = 1$, $n = 1$, where it approaches zero.

Finally, we introduce the holograms obtained for each case after the implementation of the Gerchberg-Saxton algorithm, that is, the resulting phase distribution on the EP plane (Figure 6).

The necessary parameters have been considered for implementation in a super-resolution microscope. However, due to technical issues with the microscope itself and unrelated to this study, implementation was not possible. Nevertheless, everything indicates that it is fully implementable experimentally.

It should be noted that a reduced number of pixels (128×128) was used to verify that the holograms can

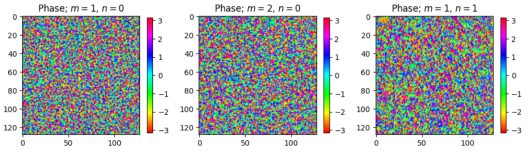

FIG. 6: Holograms obtained for each of the studied cases in Section III after the implementation of the Gerchberg-Saxton algorithm.

be implemented on a commercial SLM with modest resolution, confirming that the pixel number does not constitute a problem.

V. CONCLUSIONS

In this project, we have investigated the convergence of a modified Gerchberg-Saxton algorithm applied to three different Laguerre-Gaussian beams whose electric field components are defined by Eq. (4) to generate holograms by imposing the relative phase between the two components of the electric field in the diffraction plane and controlling the amplitude (intensity) in both the EP and the diffraction planes, leaving the global phase as a degree of freedom.

Throughout the paper, we have determined the reconstruction of the two predefined intensity profiles (one for each electric field component) as the imposed relative phase between them.

After implementing the GS algorithm, we observed that the obtained patterns reconstruct the profile of the target beam. However, they do not perfectly match due to the presence of speckle noise. In terms of the phase, it converges toward our initial conditions as it has a tendency to the imposed polarization in each case. The regions where the intensity is relevant of the reconstructed images have the expected behavior. However, there are areas where the relative phase condition is not achieved. This occurs in regions where one of the electric field components is near zero and the relative phase between them becomes undefined.

To further study the effectiveness of our approach, we have studied both the similarity (for the x and y components) and the averaged phase error, ϵ. Although the similarity values remain small, indicating little similitude between the target and reconstructed images because of the presence of noise, we obtain convergence after the second iteration of the algorithm, with values that oscillate in a small range.

Acknowledgments

First, I would like to thank my advisor, David Maluenda, for all his support, guidance, and the time he spent making this project possible. I would also like to thank him for his trust in me giving me this project and allowing me the opportunity to explore things I didn't expected.

I would also like to thank my parents, who have supported me throughout this journey and in all decisions related to my future. I would also like to thank my entire family for all the help given and the lessons I have learned from them.

Finally, I would like to thank everyone who has contributed to making this city feel like home and to all those who have read and reread these pages with me.

[1] Hariharan, P. "Basics of Holography". Cambridge University Press (2002).
[2] Slinger, Ch.; Cameron, C.; & Stanley, M. "Computer-Generated Holography as a Generic Display Technology." Computer 38, 46-53 (2005).
[3] Gerchberg, R. W.; & Saxton, W. O. "A practical algorithm for the determination of the phase from image and diffraction plane pictures." Optik 35, 237-246 (1972).
[4] Kress, B. C.; & Meyrueis, P. "Applied Digital Optics: From Micro-Optics to Nanophotonics" (Wiley, 2009).
[5] Bauchert, K.; Serati, S. K.; & Furman, A. "Advances in liquid crystal spatial light modulators," Proc. SPIE 4734, 1–10 (2002).
[6] Yang, X.; Zhao, H.; Zhang, J.; & Lu, Y. "A review of liquid crystal spatial light modulators: devices and applications," Opto-Electron. Sci. 2(8), 230026 (2023).
[7] Zhan, Q. "Cylindrical vector beams: from mathematical concepts to applications." Adv. Opt. Photon. 1, 1-57 (2009).
[8] Hell, S. W. "Far-field optical nanoscopy." Science 316, 1153–1158 (2007).
[9] Brzobohatý, O., et al. "Experimental demonstration of optical transport, sorting, and self-arrangement using a 'tractor beam'." Nat. Photonics 7, 123–127 (2013).
[10] Doster, T.; & Watnik, A. T. "Laguerre–Gauss and Bessel–Gauss beams propagation through turbulence: analysis of channel efficiency." Appl. Opt. 55, 10239–10246 (2016).
[11] Pachava, S.; Dixit, A.; & Srinivasan, B. "Modal decomposition of Laguerre Gaussian beams with different radial orders using optical correlation technique." Opt. Express 27, 13182–13193 (2019).
[12] Pang, H.; Liu, W.; Cao, A.; & Deng, Q. "Speckle-reduced holographic beam shaping with modified Gerchberg–Saxton algorithm." Optics Communications, 433, 44-51 (2019).
[13] Collett, E. "Field Guide to Polarization". SPIE Press, Bellingham, WA (2005).
[14] Wang, Z.; Bovik, A. C.; Sheikh, H. R.; & Simoncelli, E. P. "Image quality assessment: from error visibility to structural similarity." IEEE Trans. Image Process. 13, 600-612 (2004).

Algorisme Gerchberg-Saxton modificat per a generar feixos vectorials

Author: Inés Fernández Menéndez, ifername10@alumnes.ub.edu
Facultat de Física, Universitat de Barcelona, Diagonal 645, 08028 Barcelona, Spain.

Advisor: David Maluenda Niubó, dmaluenda@ub.edu

Resum: Aquest estudi explora la generació de feixos vectorials utilitzant un algorisme Gerchberg-Saxton modificat (GS) en el context de l'holografia generada per ordinador (CGH). L'objectiu és reconstruir dos components de camp elèctric ortogonals amb perfils d'intensitat predefinits i distribució de fase relativa entre components. La metodologia consisteix a aplicar l'algorisme GS de manera independent a cada component, alhora que s'imposa la seva fase relativa, permetent que la fase global evolucioni lliurement. Els feixos vectorials generats son feixos de Laguerre-Gauss amb càrregues topològiques variables, i els hologrames es calculen per a tres casos diferents. Els resultats mostren una convergència exitosa a les regions centrals dels feixos i amb presencia de soroll tipus "speckle". El patró de polarització segueix el comportament esperat, el que significa que la fase relativa està ben reconstruïda. Mètriques com la similitud i l'error de fase confirmen la convergència de l'algorisme. Aquests resultats comproven la viabilitat del mètode a implementar experimentalment, ja que es calculen segons les condicions del laboratori.
Paraules clau: Algorisme de Gerchberg-Saxton, holografia generada per ordinador, polarització, recuperació de la fase.
ODSs: Aquest TFG està relacionat amb els Objectius de Desenvolupament Sostenible ODS 4

Objectius de Desenvolupament Sostenible (ODSs o SDGs)

1. Fi de la es desigualtats		10. Reducció de les desigualtats	
2. Fam zero		11. Ciutats i comunitats sostenibles	
3. Salut i benestar		12. Consum i producció responsables	
4. Educació de qualitat	X	13. Acció climàtica	
5. Igualtat de gènere		14. Vida submarina	
6. Aigua neta i sanejament		15. Vida terrestre	
7. Energia neta i sostenible		16. Pau, justícia i institucions sòlides	
8. Treball digne i creixement econòmic		17. Aliança pels objectius	
9. Indústria, innovació, infraestructures			

Aquest TFG, part d'un grau universitari de Física, es relaciona amb l'ODS 4. En particular amb la fita 4.3 i 4.4, ja que contribueix a l'educació a nivell universitari amb igualtat d'accés per a dones i homes.